

## Two-dimensional electron gas at the AlGaIn/GaN interface

### *Layer thickness dependence*

Popok, Vladimir; Caban, Piotr; Michalowski, Pawel Piotr; Thorpe, Ryan; Feldman, Leonard; Pedersen, Kjeld

*Published in:*  
Journal of Applied Physics

*DOI (link to publication from Publisher):*  
[10.1063/1.5142766](https://doi.org/10.1063/1.5142766)

*Publication date:*  
2020

*Document Version*  
Accepted author manuscript, peer reviewed version

[Link to publication from Aalborg University](#)

### *Citation for published version (APA):*

Popok, V., Caban, P., Michalowski, P. P., Thorpe, R., Feldman, L., & Pedersen, K. (2020). Two-dimensional electron gas at the AlGaIn/GaN interface: Layer thickness dependence. *Journal of Applied Physics*, 127(11), Article 115703. <https://doi.org/10.1063/1.5142766>

### **General rights**

Copyright and moral rights for the publications made accessible in the public portal are retained by the authors and/or other copyright owners and it is a condition of accessing publications that users recognise and abide by the legal requirements associated with these rights.

- Users may download and print one copy of any publication from the public portal for the purpose of private study or research.
- You may not further distribute the material or use it for any profit-making activity or commercial gain
- You may freely distribute the URL identifying the publication in the public portal -

### **Take down policy**

If you believe that this document breaches copyright please contact us at [vbn@aub.aau.dk](mailto:vbn@aub.aau.dk) providing details, and we will remove access to the work immediately and investigate your claim.

## Two dimensional electron gas at the AlGa<sub>N</sub>/Ga<sub>N</sub> interface: layer thickness dependence

Vladimir N. Popok<sup>1,a)</sup> Piotr A. Caban<sup>2</sup>, Pawel Piotr Michalowski<sup>2</sup>, Ryan Thorpe<sup>3</sup>, Leonard C. Feldman<sup>3</sup>, and Kjeld Pedersen<sup>1</sup>

### AFFILIATIONS

<sup>1</sup> Department of Materials and Production, Aalborg University, 9220 Aalborg, Denmark

<sup>2</sup> Institute of Electronic Materials Technology, 01-919 Warsaw, Poland

<sup>3</sup> Department of Physics & Astronomy, Rutgers The State University of New Jersey, Piscataway, New Jersey 08854, USA

<sup>a)</sup> Electronic mail: vp@mp.aau.dk

### ABSTRACT

In the current paper, structure and properties of the AlGa<sub>N</sub>/Ga<sub>N</sub> interfaces are studied, explaining the role of AlGa<sub>N</sub> layer thickness on the two-dimensional electron gas (2DEG) formation. It is found that the generation of a continuous electron gas requires AlGa<sub>N</sub> films with stable stoichiometry, which can be reached only above a certain critical thickness,  $\approx 6\text{-}7$  nm in our case (20 at. % Al content). Thinner films are significantly affected by the oxidation, which causes composition variations and structural imperfections leading to an inhomogeneity of the polarization field and, as a consequence, of the electron density across the interface. Using Kelvin probe force microscopy, this inhomogeneity can be visualized as variations of the surface potential on the sub-micron scale. For the heterostructures with layer thickness above the critical value, the surface potentials maps become homogeneous, reflecting a weakening influence of the oxidation on the interface electronic properties. The 2DEG formation is confirmed by the Hall measurements for these heterostructures.

## I. INTRODUCTION

The wide bandgap semiconductor GaN provides attractive properties such as high breakdown field, high thermal conductivity and high charge carrier velocity making it of great interest for power switching devices [1, 2]. An additional desirable aspect is the formation of a two-dimensional electron gas (2DEG) at the interface with another III-N semiconductor, typically AlGaN, enabling fabrication of high electron mobility transistors [3-6]. In the last decade, such heterostructures, possessing 2DEG, are also in high demands for applications in THz electronics [7, 8].

At the epitaxially grown AlGaN/GaN interface, the lattice mismatch and difference in coefficients of thermal expansion (CTE) lead to strain formation. Since nitride semiconductors lack a centre of inversion symmetry, the presence of strain causes piezoelectric polarization. Additionally, there is a spontaneous polarization due to the difference in electronegativity of these III-N materials. In the case of Ga-faced GaN buffer with top AlGaN layer, the total polarization causes positive net charge on the AlGaN side requiring “negative” compensation from GaN in the form of 2DEG [9] which is associated with the donor-like surface states [10].

For device fabrication, GaN is typically grown as a micron thick film on substrates of sapphire, silicon or silicon carbide. Due to the lattice and CTE mismatches, the synthesised GaN films suffer from a high concentration of threading dislocations (TD), which also affects the crystalline quality of the epitaxial AlGaN layer grown on the top and properties of the 2DEG at the interface [11-14]. In addition to crystallinity, one needs to consider composition (Al-content  $x$ ,  $\text{Al}_x\text{Ga}_{1-x}\text{N}$ ) and layer thickness. Both parameters are found to affect charge carrier concentration and mobility [4, 15]. Increase in  $x$ , on the one hand, facilitates higher electron concentration due to stronger polarization fields at the interface but, on the other hand, increases the lattice mismatch causing higher strain impairing the electron mobility. To reach a compromise, Al content is suggested to be optimal in the 20-30% range [16-18]. There are also several practical reasons to control AlGaN thickness, which affects the gate leakage current, Schottky barrier at metal electric contacts and 2DEG parameters [19-21]. It was found that a critical (minimal) thickness of AlGaN layer is required in order to initiate the 2DEG. The further thickness increase affects both the electron density and mobility but with opposite tendencies: the former increases while the latter decreases with the thickness [15]. These tendencies again require a compromise yielding a rather narrow thickness interval, typically between 15-30 nm [16-18, 21]. Nevertheless, the issue of critical thickness is

rather poorly studied. The available publications about the critical thickness of AlGa<sub>N</sub> report that a layer of 4-6 nm is needed in order to enable 2DEG formation [10, 22]. A correlated finding was reported in [23], where no 2DEG formation was observed for Al<sub>0.25</sub>Ga<sub>0.75</sub>N layer with thickness of 3 nm. To our knowledge there are no models explaining physical reasons for the critical thickness and no reports on the dynamics of 2DEG formation under a thickness transition from below to above a critical value.

In the current paper, we present the results on studies of thin (from ca. 2 to 12 nm) layers of AlGa<sub>N</sub> grown on Ga<sub>N</sub> in order to evaluate critical thickness for 2DEG nucleation and bring new insights into dynamics of the electron gas formation.

## II. SAMPLE GROWTH AND EXPERIMENTAL METHODS

AlGa<sub>N</sub>/Ga<sub>N</sub> heterostructures were grown on 2-inch single side polished (0001)-oriented sapphire substrates with a maximum miscut of 0.2° to the m-plane. The synthesis was performed using an AIX 200/4 RF-S metal-organic chemical vapour deposition low-pressure reactor utilizing source gases of trimethylaluminium, trimethylgallium, ammonia and hydrogen as carrier gas. The reactor parameters (pressure, temperature and gas fluxes) for all III-N fabricated layers were very similar to those described in [11]. Growth was carried out by: formation of a thin AlN nucleation (low-temperature) layer; further growth at higher temperature yielding in total 745±15 nm thick AlN film; and a 1090±150 nm thick Ga<sub>N</sub> buffer synthesis. These thicknesses were established via cross-sectional scanning electron microscopy. One of the Ga<sub>N</sub> wafers is used as a reference sample while layers of increasing thickness of AlGa<sub>N</sub> are fabricated on another six wafers (samples 1 to 6) [keeping the same synthesis parameters except the growth time of the top layer](#).

Evaluation of the composition and thickness of these nanometer thin layers was carried out by secondary ion mass spectroscopy (SIMS), X-ray photoelectron spectroscopy (XPS) assisted by sputtering and transmission electron microscopy (TEM). SIMS measurements were performed employing the CAMECA SC Ultra instrument under ultra-high vacuum conditions of  $4 \times 10^{-10}$  mbar. Sufficient depth resolution was obtained for negative ion detection mode using a Cs<sup>+</sup> primary beam with energy of 150 eV allowing to analyse 200×200 μm<sup>2</sup> areas. TEM measurements were carried out by the Philips EM420 microscope at an accelerating voltage of 100 kV. For X-ray photoelectron spectroscopy (XPS) measurements, a Thermo Scientific K-Alpha spectrometer was utilized. The X-ray beam was produced by a monochromated Al Kα source with an energy of

1486.6 eV. The total instrumental resolution was 0.5 eV. In order to avoid charging during the measurements, a low energy dual beam  $\text{Ar}^+$  and electron flood gun was directed at the sample. The binding energy of the peaks was calibrated using the main component of the adventitious carbon peak at 284.8 eV. In order to determine the composition of the films as a function of depth, ion beam etching was performed in 10 second increments using 1 keV  $\text{Ar}^+$  ions which removed about 0.3 nm of AlGaIn per cycle. Hall and Kelvin probe force microscopy (KPFM) measurements were used to determine the properties of the 2DEG. Electrical parameters were obtained using the van der Pauw method. The AlGaIn/GaN heterostructures were prepared in square shapes ( $7 \times 7 \text{ mm}^2$ ) with contacts made of pure indium 6N and placed in the corners. Measurements were carried out in a magnetic field of 1 T at room (300 K) and liquid nitrogen (77 K) temperatures using a system composed of Keithley units (model 7065 card, DC power supply model 6221, nanovoltmeter model 2182) and triaxial cables, which together provided a very high input resistance ( $10^{12} \Omega$ ) and high accuracy in voltages measurements. The KPFM was performed using Ntegra-Aura nanolaboratory and two-pass technique described in detail elsewhere [24]. Commercial silicon cantilevers with gold conductive coating (tip curvature radius  $\leq 35 \text{ nm}$ ) were used providing a lateral resolution of KPFM images better than 100 nm.

### III. RESULTS AND DISCUSSION

Depth profiles obtained by SIMS (Fig. 1a) show the presence of oxygen in a thin surface layer indicative of oxidation of Al and Ga. The intense peaks of Al and Ga within the first nanometer of the layer are artefacts associated with the increased sputtering efficiency and enhanced charge states due to the presence of oxide. Similar surface peaks of Al and Ga are found on all studied samples. *For this reason, it became impossible to obtain a reliable depth profile for sample 1 with the thinnest AlGaIn layer. For samples 2-5, the Al and Ga profiles become constant at higher depth indicating the formation of AlGaIn films with stable stoichiometry. Thereafter, the Al concentration decreases while Ga concentration rises to the next constant value indicating transition to pure GaN. This transition occurs on the length scale of about 2 nm. Thus, monitoring the Al profiles (see Fig. 1b) allows an estimate of the thicknesses of top AlGaIn layers as presented in Tab. 1. Fig. 1b also shows that the Al concentration is the same in all grown layers, indicative of a stable AlGaIn stoichiometry from sample to sample.*

Using XPS, concentrations of Al, Ga and N are found by evaluation of Al 2p, Ga 3d and N 1s peaks (see Fig. 2). The Ga 3d spectrum exhibits several sets of doublets, indicating the presence of elemental Ga and oxidized AlGa<sub>N</sub> as well as stoichiometric AlGa<sub>N</sub>. The presence of oxide is consistent with the SIMS results. Unfortunately, the peak N 1s cannot be precisely deconvoluted and quantified because of its overlap with the Ga LMM (Auger) peak. This uncertainty in the nitrogen content affects the precision of Al and Ga concentration calculation. The results for Al are presented in Tab. 1 yielding the values between 18-21 at. % for samples 3-6. Note that the Al percentage measured for samples 1 and 2 is lower due to the contribution of the underlying Ga<sub>N</sub>. The AlGa<sub>N</sub> layers of these samples are so thin that the photo-excited electrons are also detected from the Ga<sub>N</sub> buffer, thus, artificially decreasing the real Al/Ga ratio in AlGa<sub>N</sub>. However, taking into consideration the SIMS spectra presented in Fig. 1b, which show the same Al concentration for samples 2-5, we can disregard this artefact and conclude that Al content is the same in all samples, i.e. approximately 20 at. %.

XPS measurements were also carried out in combination with the sputtering of AlGa<sub>N</sub> films. Fig. 3 shows a decrease of Al 2p peak intensity with sputtering time for sample 2. Assuming the same sputtering coefficient for all films in question, the thickness of the Al containing layer can be found. These data are added to Tab. 1 showing a reasonable agreement with the values obtained by SIMS for samples 2-4. For samples 5 and 6, ion beam mixing of atoms in the film and bulk made the XPS thickness measurements unreliable, and the film thicknesses were estimated from SIMS and TEM, respectively. The TEM image of sample 6 is shown in Fig. 4.

For heterostructures with AlGa<sub>N</sub> thickness  $\leq 5$  nm (samples 1-3) Hall measurements showed resistance  $\rho$  on MOhm scale, thus, yielding very low charge carrier concentration  $n$  and electron mobility  $\mu$ , suggesting that there is no continuous 2DEG formed across the interface. For sample 4 with a  $\approx 7$  nm thick AlGa<sub>N</sub> layer,  $\rho$  drops to kOhm level yielding  $n = 1.35 \times 10^{12} \text{ cm}^{-2}$  and  $\mu = 403.6 \text{ cm}^2/\text{Vs}$  at room temperature (Tab. 2). Measurements at 77K show lower resistance and higher carrier concentration and mobility, as expected. Slight increase of AlGa<sub>N</sub> thickness (sample 5) leads to increase of both  $n$  and  $\mu$ . For sample 6, with a  $\approx 12$  nm thick AlGa<sub>N</sub> layer, the carrier concentration further increases while the mobility decreases. The decrease is particularly high (more than 2 times) at low temperature. This tendency is in good agreement with the one found in [15] indicating that the thicker layer introduces higher stress, thus, decreasing the crystalline quality at the interface and increasing scattering of the charge carriers.

Topography of the reference (GaN) sample can be seen in Fig. 5a. The AFM image shows a typical surface texture with terraces. The height variations across the surface reach approximately 7 nm yielding a root mean square roughness value of 1.3 nm. AlGa<sub>N</sub> layers epitaxial grown on top of GaN follow its topography (not shown) and have very similar roughness values. TDs formed in GaN are terminated at the surface as small conical in shape pits known as V-defects [11, 25, 26]. In Fig. 5c these defects are visible as black dots. The surface density is calculated to be  $(2.5 \pm 0.7) \times 10^9 \text{ cm}^{-2}$ . The analysis of sample 1 (with the thinnest AlGa<sub>N</sub> layer) and 5 (the second thickest layer) both show the value of  $\approx 3.0 \times 10^9 \text{ cm}^{-2}$ , which is essentially the same (within the standard deviation) as for the reference sample indicating that the TDs formed in GaN are transferred into the AlGa<sub>N</sub> epilayers.

KPFM yields the contact potential difference (CPD) between the tip and surface. For the GaN sample, CPD is measured at different surface positions and the mean value is calculated to be  $0.72 \pm 0.02 \text{ V}$ . Ideally, this value indicates the work function difference of the tip and sample materials. However, the measurements are done in air and we can not exclude the presence of a thin liquid layer (due to humidity) on the surface which can affect the measured CPD. The map of potential variations in Fig. 5b shows a very homogeneous distribution across the surface supporting the assumption of homogeneity of the electronic properties (electron density) in a top GaN layer.

KPFM images of the samples with AlGa<sub>N</sub> films presented in Fig. 6 show distinct changes compared to GaN. The mean CPD values given in Tab. 3 are much greater than that of GaN. This is expected as the band gap of AlGa<sub>N</sub> is larger than that of GaN while the electron affinity is smaller, ca. 2.5 eV for Al<sub>0.2</sub>Ga<sub>0.8</sub>N compared to 3.3 eV for GaN [27]. This implies a larger difference between the work function of the tip (Au in both case) and Al<sub>0.2</sub>Ga<sub>0.8</sub>N compared to GaN. The images for samples 1-3 (panels (a-c) of Fig. 6) show highly inhomogeneous, “mosaic-like” potential distributions across the studied areas. The deviations for mean CPD value (see Tab. 3) are also high. The observed inhomogeneity reflects variations of electronic properties of the AlGa<sub>N</sub> layer and interface with GaN. Reasons for these variations can be local fluctuations of Al concentration and surface reconstruction caused by the oxide layer formation [28], which is found by SIMS in our case. These effects should be especially pronounced for the thinner layers. For example, in sample 2 the AlGa<sub>N</sub> layer thickness is around 3.5 nm, which is equivalent of 7 unit cells (lattice parameter  $c$  is 0.5185 nm for GaN and 0.4980 nm for AlN in the wurtzite structure).

Oxygen is found to the depth of 1.0 nm (Fig. 1b). Thus, at least 2 unit cells of AlGa<sub>N</sub> in thickness should be corrupted by oxygen. Similar, but less pronounced effects, can be expected for sample 3, with thickness equivalent to 10 unit cells, while it should be a very large effect for sample 1 with the layer thickness equivalent of only 3 unit cells.

Variations of Al concentration cause alterations of spontaneous polarization, while the reconstruction of crystalline structure affects piezoelectric polarization. Local changes of the polarization field influence the interface net charge and electron density, thus, they can be the origin of the “mosaic-like” maps of surface potential (Fig. 6a-c). In Hall measurements, we found very high resistivity for these samples. Thus, we can conclude that there is no continuous electron gas formed at the interface if the AlGa<sub>N</sub> layer is below a critical thickness. Increasing layer thickness (samples 4-6), reveals a transition to more homogeneous surface potential maps (see Fig. 6d-f). For these samples, the surface phenomena (oxidation, Al concentration variations, crystalline imperfections) affect the homogeneity of polarization field at the interface to a lesser extent facilitating the formation of quasi-continuous or continuous 2DEG, which is consistent with the Hall measurements (see Tab. 2). Hence, it can be concluded that a transition from a “mosaic-like” to homogeneous KPFM images correlates well with the formation of 2DEG. Based on the obtained results, we suggest a critical thickness of AlGa<sub>N</sub> layer for the 2DEG formation to be approximately 6-7 nm for 20 at. % of Al.

It is worth mentioning that a similar evolution from an island-like to homogeneous surface potential distribution was found by KPFM for LaAlO<sub>3</sub>/SrTiO<sub>3</sub> heterostructures [24], which are also known for 2DEG generation at the interface. The studies [29] revealed that Al concentration in the surface layers of LaAlO<sub>3</sub> with a thickness below the critical value is not stable across the surface, and the surface potential inhomogeneity observed by KPFM reflects these variations of composition though the local alterations of electron density. Transition to the stable stoichiometry, occurring above the certain critical thickness of the LaAlO<sub>3</sub>, was found to be in good agreement with the evolution towards homogeneous surface potential maps and was attributed to quasi-continuous 2DEG generation. Similar to our case, presence of extrinsic defects in the LaAlO<sub>3</sub> film was found to be the main reason significantly affecting the interface conductivity [30].



#### IV. CONCLUSION

The 2DEG at the interface between AlGaIn layer and GaN buffer is studied and a physical model explaining the role of the layer thickness on the electron gas formation is suggested. It is found that the AlGaIn layers thinner than approximately 6-7 nm are significantly affected by the surface oxidation, which causes variations in composition and crystalline structure and, hence, lead to the strong inhomogeneity of the polarization field at the interface. This inhomogeneity affects the density of electrons attracted to the interface and can be visualized as variations of the surface potential on the sub-micron scale in the KPFM images. With increasing layer thickness, the measured surface potential maps become more homogeneous reflecting the effects of weakening of surface oxidation and reconstruction on the interface electronic properties. Above a critical thickness, which is found for our heterostructures (20 at. % of Al) to be  $\approx$  6-7 nm, KPFM represents a relatively homogeneous potential distribution across the surface and Hall measurements show the electrical parameters (carrier concentration and mobility) consistent with 2DEG formation.

#### ACKNOWLEDGEMENTS

The authors would like to thank Dr. Søren Nielsen from Aarhus University for the help with TEM measurements. We also acknowledge the financial support from the Innovation Fund Denmark under the project “Semiconductor materials for power electronics - SEMPEL”.

#### REFERENCES

- <sup>1</sup> J. Millan, P. Godignon, X. Perpina, A. Perez-Tomas, and J. Rebollo, IEEE Trans. Power Electron. **29**, 2155 (2014).
- <sup>2</sup> D. Shahin and A. Christou, ECS Trans. **64**, 203 (2014).
- <sup>3</sup> E.T. Yu, G.J. Sullivan, P.M. Asbeck, C.D. Wang, D. Qiao, and S.S. Lau, Appl. Phys. Lett. **71**, 2794 (1997).
- <sup>4</sup> O. Ambacher, J. Smart, J. R. Shealy, N. G. Weimann, K. Chu, M. Murphy, W. J. Schaff, L. F. Eastman, R. Dimitrov, L. Wittmer, M. Stutzmann, W. Rieger, and J. Hilsenbeck, J. Appl. Phys. **85**, 3222 (1999).
- <sup>5</sup> F. Zeng, J. Xilin An, G. Zhou, W. Li, H. Wang, T. Duan, L. Jiang, and H. Yu, Electronics **7**, 377 (2018).

- <sup>6</sup> J. Bergsten, J.-T. Chen, S. Gustafsson, A. Malmros, U. Forsberg, M. Thorsell, E. Janzen, and N. Rorsman, *IEEE Transact. Electron. Dev.* **63**, 333 (2016).
- <sup>7</sup> K. Ahi, *Opt. Eng.* **56**, 090901 (2017).
- <sup>8</sup> H.W. Hou, Z. Liu, J.H. Teng, T. Palacios, and S.J. Chua, *Sci. Rep.* **7**, 46664 (2017).
- <sup>9</sup> H. Morkoc, *Handbook of nitride semiconductors and devices*, Vol. 1, Weinheim: Wiley-VCH, 2008.
- <sup>10</sup> J.P. Ibbetson, P.T. Fini, K.D. Ness, S.P. DenBaars, J.S. Speck, and U.K. Mishra, *Appl. Phys. Lett.* **77**, 250 (2000).
- <sup>11</sup> V.N. Popok, T.S. Aunsborg, R.H. Godiksen, P.K. Kristensen, R.R. Juluri, P. Caban, and K. Pedersen, *Rev. Adv. Mater. Sci.* **57**, 72 (2018).
- <sup>12</sup> S.W. Kaun, M.H. Wong, U.K. Mishra, and J.S. Speck, *Appl. Phys. Lett.* **100**, 262102 (2012).
- <sup>13</sup> D. Christy, A. Watanabe, and T. Egawa, *AIP Adv.* **4**, 107104 (2014).
- <sup>14</sup> M.J. Manfa, N. G. Weimann, J. W. P. Hsu, L. N. Pfeiffer, K. W. West, and S.N.G. Chu, *Appl. Phys. Lett.* **81**, 1456 (2002).
- <sup>15</sup> S. Heikman, S. Keller, Y. Wu, J.S. Speck, S.P. DenBaars, and U.K. Mishra, *J. Appl. Phys.* **93**, 10114 (2003).
- <sup>16</sup> I. Khalil, E. Bahat-Treidel, F. Schnieder, and J. Wurfl, *IEEE Trans. Electron. Dev.* **56**, 361 (2009).
- <sup>17</sup> X. Wang, S. Huang, Y. Zheng, K. Wei, X. Chen, H. Zhang, and X. Liu, *IEEE Trans. Electron. Dev.* **61**, 1341 (2014).
- <sup>18</sup> A. Goyal, B.S. Yadav, R. Raman, and A.K. Kapoor, *AIP Adv.* **8**, 025021 (2018).
- <sup>19</sup> S. Turuvekere, A. DasGupta, and N. DasGupta, *IEEE Trans. Electron. Dev.* **62**, 3449 (2015).
- <sup>20</sup> Y. Takei, K. Tsutsui, W. Saito, K. Kakushima, H. Wakabayashi, and H. Iwai, *Jap. J. Appl. Phys.* **55**, 040306 (2016).
- <sup>21</sup> V.G. Tikhomirov, V.E. Zemlyakov, V.V. Volkov, Ya.M. Parnes, V.N. Vyuginov, W.V. Lundin, A.V. Sakharov, E.E. Zavarin, A.F. Tsatsulnikov, N.A. Cherkashin, M.N. Mizerov, and V.M. Ustinov, *Semiconductors* **50**, 244 (2016).
- <sup>22</sup> Y. Zhang, I. P. Smorchkova, C. R. Elsass, S. Keller, J.P. Ibbetson, S. Denbaars, U.K. Mishra, and J. Singh, *J. Appl. Phys.* **87**, 7981 (2000).
- <sup>23</sup> R. Brown, D. Macfarlane, A. Al-Khalidi, X. Li, G. Ternent, H. Zhou, I. Thayne, and E. Wasige, *IEEE Electron. Dev. Lett.* **35**, 906 (2014).

This is the author's peer reviewed, accepted manuscript. However, the online version of record will be different from this version once it has been copyedited and typeset.  
PLEASE CITE THIS ARTICLE AS DOI: 10.1063/1.5142766

- <sup>24</sup> V.N. Popok, A. Kalabukhov, R. Gunnarsson, S. Lemesko, T. Claeson, and D. Winkler, J. Adv. Microsc. Res. **5**, 26 (2010).
- <sup>25</sup> P. Gibart, Rep. Prog. Phys. **67**, 667 (2004).
- <sup>26</sup> L. Zhang, K.H. Lee, I.M. Riko, C.-C. Huang, A. Kadir, K.E. Lee, S.J. Chua, and E.A. Fitzgerald, Semicond. Sci. Technol. **32**, 065001 (2017).
- <sup>27</sup> S.P. Grabowski, M. Schneider, H. Nienhaus, W. Mönch, R. Dimitrov, O. Ambacher, and M. Stutzmann, Appl. Phys. Lett. **78**, 2503 (2001).
- <sup>28</sup> M.S. Miao, J.R. Weber, and C.G. Van de Walle, J. Appl. Phys. **107**, 123713 (2010).
- <sup>29</sup> A.S. Kalabukhov, Yu.A. Boikov, I.T. Serenkov, V.I. Sakharov, V.N. Popok, R. Gunnarsson, J. Börjesson, N. Ljustina, E. Olsson, D. Winkler, and T. Claeson, Phys. Rev. Lett. **103**, 146101 (2009).
- <sup>30</sup> M.P. Warusawithana, C. Richter, J.A. Mundy, P. Roy, J. Ludwig, S. Paetel, T. Heeg, A.A. Pawlicki, L.F. Kourkoutis, M. Zheng, M. Lee, B. Mulcahy, W. Zander, Y. Zhu, J. Schubert, J.N. Eckstein, D.A. Muller, C. Stephen Hellberg, J. Mannhart, and D.G. Schlom, Nature Commun. **4**, 2351 (2013).

## Tables

Table 1. Al concentration calculated from XPS data and thickness of AlGaIn films found by different methods indicated in parentheses.

Sample No.	Al, at. %	Thickness, nm
1	7	1.6(XPS)
2	15	3.8(SIMS) 3.3(XPS)
3	20	5.2(SIMS) 4.9(XPS)
4	20	6.5(SIMS) 7.3(XPS)
5	18	7.8(SIMS)
6	21	12.5(TEM)

Table 2. Contact resistance, charge carrier concentration and mobility measured by Hall method at room temperature and 77 K.

Sample	AlGaIn thickness, nm	$T$ , K	$\rho$ , kOhm/cm <sup>2</sup>	$n$ , 10 <sup>12</sup> cm <sup>-2</sup>	$\mu$ , cm <sup>2</sup> /Vs
4	$\approx 7$	300	11.49	1.35	403.6
		77	0.97	2.65	2422.1
5	$\approx 8$	300	3.45	2.36	765.8
		77	0.24	4.05	6298.7
6	$\approx 12$	300	2.38	4.56	575.4
		77	0.50	4.40	2862.7

Table 3. Measured CPD values for samples 1-6.

Sample	1	2	3	4	5	6
CPD, V	1.26 $\pm$ 0.05	1.24 $\pm$ 0.03	1.23 $\pm$ 0.03	1.20 $\pm$ 0.02	1.25 $\pm$ 0.01	1.22 $\pm$ 0.01

### Figure captions

Fig. 1. SIMS depth profiles (a) of oxygen, aluminium and gallium in sample 5 and (b) of aluminium in samples 2 to 5 corresponding to increasing thickness of AlGa<sub>N</sub> layer. Dashed vertical lines in panel (b) show concentration cut-off corresponding to decrease for one order of magnitude.

Fig. 2. Measured XPS spectral elements corresponding to Al 2p, Ga 3d and N 1s, (dot curves with blue fits) with corresponding convolution plots for different components highlighted in different colours. Red plots correspond to stoichiometric AlGa<sub>N</sub>. In Al and Ga panels, two red curves reflect doublets due to the spin-orbit splitting. In Ga panel, blue plots correspond to oxidized AlGa<sub>N</sub>/Ga<sub>N</sub>, yellow one to possibly of N deficient AlGa<sub>N</sub>/Ga<sub>N</sub> and orange plot to elemental Ga.

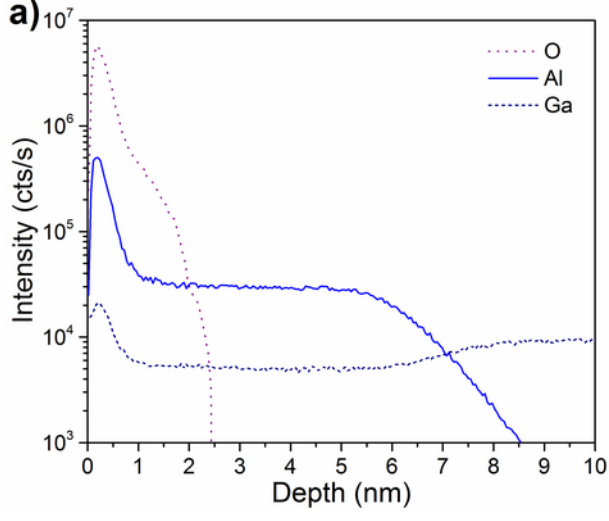
Fig. 3. Intensity decrease of Al 2p peak with increasing sputtering (etch) time for sample 2.

Fig. 4. TEM image of the AlGa<sub>N</sub>/Ga<sub>N</sub> interface (visualised by dash line) for sample 6.

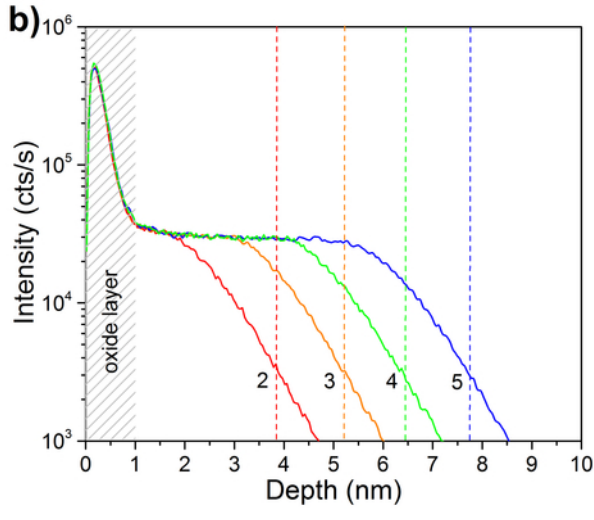
Fig. 5. (a) AFM and (b) KPFM 10×10 μm<sup>2</sup> images of Ga<sub>N</sub> surface (reference sample) as well as (c) AFM image on smaller scale of 1.5×1.5 μm<sup>2</sup> visualising V-defects (black dots).

Fig. 6. KPFM images of samples 1-6 with increasing AlGa<sub>N</sub> layer thickness: a) ≈1.5 nm, b) ≈3.5 nm, c) ≈5 nm, d) ≈7 nm, e) ≈8 nm and f) ≈12 nm.

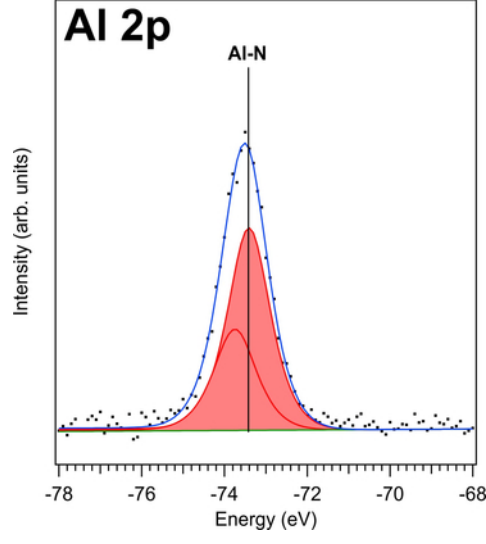
This is the author's peer reviewed, accepted manuscript. However, the online version of record will be different from this version once it has been copyedited and typeset.  
PLEASE CITE THIS ARTICLE AS DOI: 10.1063/1.5142766



This is the author's peer reviewed, accepted manuscript. However, the online version of record will be different from this version once it has been copyedited and typeset.  
PLEASE CITE THIS ARTICLE AS DOI: 10.1063/1.5142766

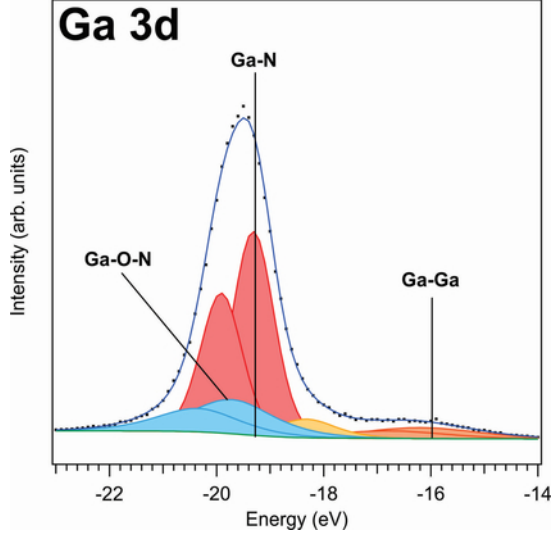


This is the author's peer reviewed, accepted manuscript. However, the online version of record will be different from this version once it has been copyedited and typeset.  
PLEASE CITE THIS ARTICLE AS DOI: 10.1063/1.5142766

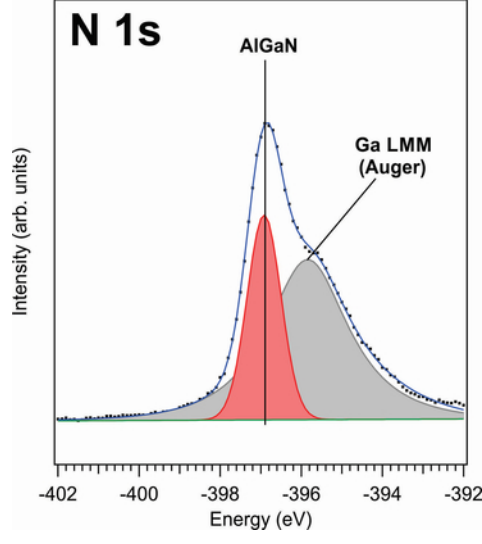




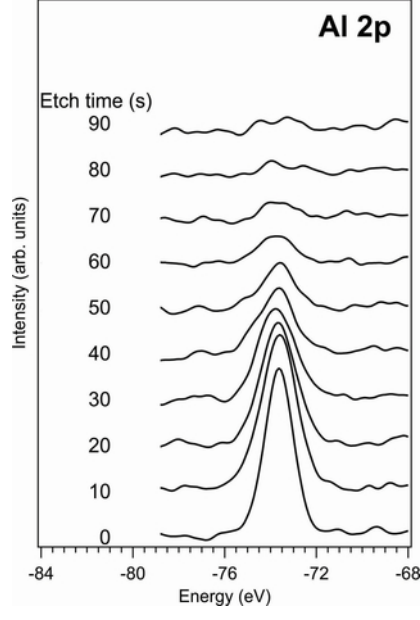
This is the author's peer reviewed, accepted manuscript. However, the online version of record will be different from this version once it has been copyedited and typeset.  
PLEASE CITE THIS ARTICLE AS DOI: 10.1063/1.5142766



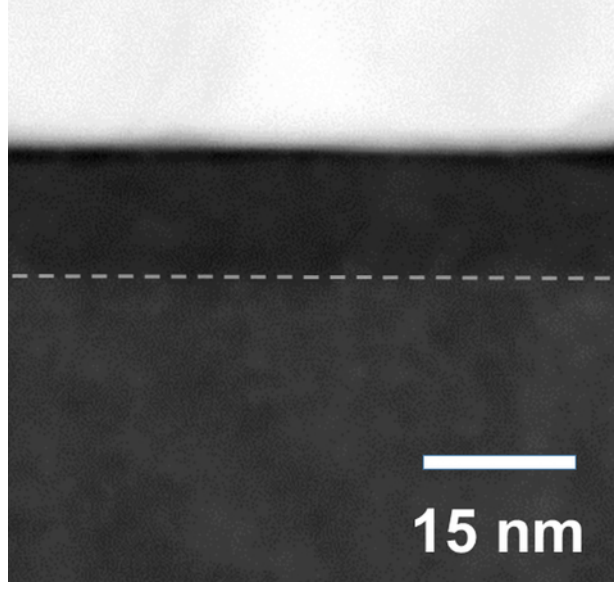
This is the author's peer reviewed, accepted manuscript. However, the online version of record will be different from this version once it has been copyedited and typeset.  
PLEASE CITE THIS ARTICLE AS DOI: 10.1063/1.5142766



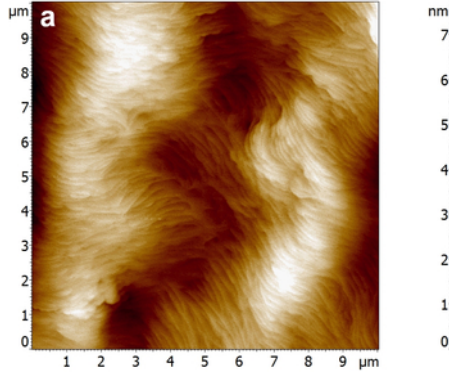
This is the author's peer reviewed, accepted manuscript. However, the online version of record will be different from this version once it has been copyedited and typeset.  
PLEASE CITE THIS ARTICLE AS DOI: 10.1063/1.5142766



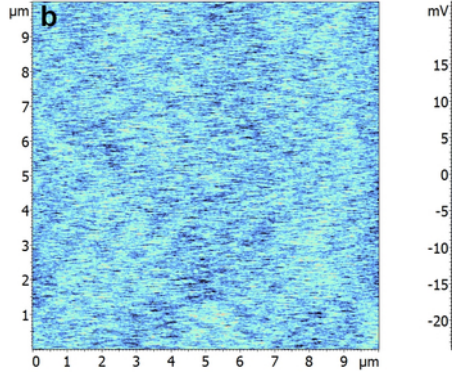
This is the author's peer reviewed, accepted manuscript. However, the online version of record will be different from this version once it has been copyedited and typeset.  
PLEASE CITE THIS ARTICLE AS DOI: 10.1063/1.5142766



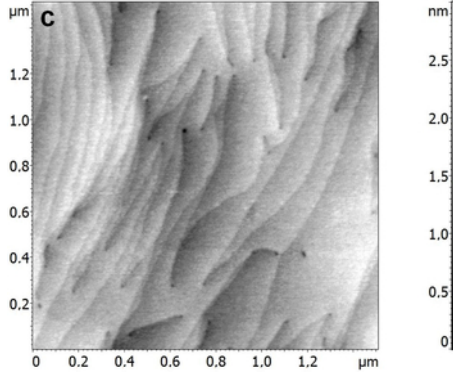
This is the author's peer reviewed, accepted manuscript. However, the online version of record will be different from this version once it has been copyedited and typeset.  
PLEASE CITE THIS ARTICLE AS DOI: [10.1063/1.5142766](https://doi.org/10.1063/1.5142766)



This is the author's peer reviewed, accepted manuscript. However, the online version of record will be different from this version once it has been copyedited and typeset.  
PLEASE CITE THIS ARTICLE AS DOI: 10.1063/1.5142766



This is the author's peer reviewed, accepted manuscript. However, the online version of record will be different from this version once it has been copyedited and typeset.  
PLEASE CITE THIS ARTICLE AS DOI: [10.1063/1.5142766](https://doi.org/10.1063/1.5142766)



This is the author's peer reviewed, accepted manuscript. However, the online version of record will be different from this version once it has been copyedited and typeset.  
PLEASE CITE THIS ARTICLE AS DOI: 10.1063/1.5142766

